AGU PUBLICATIONS

Geochemistry, Geophysics, Geosystems

RESEARCH ARTICLE
10.1002/2015GC005810

Key Points:
- Illite preserves the hydrogen isotopic signature and age of paleofluids in the earth's upper crust
- Three fluid events are pinpointed in the NAK
- The NAF exploited zones of preexisting weak clay material during its formation

Supporting Information:
- Supporting Information S1

Correspondence to:
A. Boles,
aboles@umich.edu

Citation:
Boles, A., B. van der Pluijm, A. Mulch, H. Mutlu, I. T. Uysal, and L. N. Warr (2015), Hydrogen and $^{40}Ar/^{39}Ar$ isotope evidence for multiple and protracted paleofluid flow events within the long-lived North Anatolian Keirogen (Turkey), *Geochem. Geophys. Geosyst.*, *16*, 1975–1987, doi:10.1002/2015GC005810.

Received 5 MAR 2015
Accepted 1 JUN 2015
Accepted article online 3 JUN 2015
Published online 28 JUN 2015

Hydrogen and $^{40}Ar/^{39}Ar$ isotope evidence for multiple and protracted paleofluid flow events within the long-lived North Anatolian Keirogen (Turkey)

Austin Boles[1], Ben van der Pluijm[1], Andreas Mulch[2], Halim Mutlu[3], I. Tonguç Uysal[4], and Laurence N. Warr[5]

[1]Department of Earth and Environmental Sciences, University of Michigan, Ann Arbor, Michigan, USA, [2]Senckenberg Biodiversität und Klima Forschungszentrum, Frankfurt, Germany, [3]Department of Geological Engineering, Ankara University, Ankara, Turkey, [4]Queensland Geothermal Energy Centre of Excellence, University of Queensland, St. Lucia, Queensland, Australia, [5]Ernst-Moritz-Arndt Universität Greifswald, Institut für Geographie und Geologie, Greifswald, Germany

Abstract We present a new approach to identifying the source and age of paleofluids associated with low-temperature deformation in the brittle crust, using hydrogen isotopic compositions (δD) and $^{40}Ar/^{39}Ar$ geochronology of authigenic illite in clay gouge-bearing fault zones. The procedure involves grain-size separation, polytype modeling, and isotopic analysis, creating a mixing line that is used to extrapolate to δD and age of pure authigenic and detrital material. We use this method on samples collected along the surface trace of today's North Anatolian Fault (NAF). δD values of the authigenic illite population, obtained by extrapolation, are $-89 \pm 3‰$, $-90 \pm 2‰$, and $-97 \pm 2‰$ (VSMOW) for samples KSL, RES4-1, and G1G2, respectively. These correspond to δD fluid values of $-62‰$ to $-85‰$ for the temperature range of 125°C ± 25°, indistinguishable from present-day precipitation values. δD values of the detrital illite population are $-45 \pm 13‰$, $-60 \pm 6‰$, and $-64 \pm 6‰$ for samples KSL, G1G2, and RES4-1, respectively. Corresponding δD fluid values at 300°C are $-26‰$ to $-45‰$ and match values from adjacent metamorphic terranes. Corresponding clay gouge ages are 41.4 ± 3.4 Ma (authigenic) and 95.8 ± 7.7 Ma (detrital) for sample G2 and 24.6 ± 1.6 Ma (authigenic) and 96.5 ± 3.8 Ma (detrital) for sample RES4-1, demonstrating a long history of meteoric fluid infiltration in the area. We conclude that today's NAF incorporated preexisting, weak clay-rich rocks that represent earlier mineralizing fluid events. The samples preserve at least three fluid flow pulses since the Eocene and indicate that meteoric fluid has been circulating in the upper crust in the North Anatolian Keirogen since that time.

1. Introduction

Active fault zones of the upper-crustal, brittle deformation regime are dynamic and variable environments, both spatially and temporally. Multiple parameters directly or indirectly control the morphology and character of fault zones, including wall rock lithology, three-dimensional fault geometry, rate and amount of displacement, preexisting structure, and fluid-rock interaction [e.g., *Sibson*, 1977; *Scholz*, 1987; *Bruhn et al.*, 1990; *Caine et al.*, 1996]. These primary controls determine fault zone features such as permeability and porosity structure, fluid flux, and mineralization suites, and lead to the resulting peculiarity of fault zones to behave either as fluid flow barriers or fluid flow conduits [*Oliver*, 1986; *Sibson*, 1992; *Hickman et al.*, 1995; *Person et al.*, 2007; *Sutherland et al.*, 2012]. Fault rock formation is a result of interactions between physical and chemical processes, with characteristics that evolve throughout the displacement cycle.

Recent work has highlighted the importance of low-temperature clay mineral authigenesis and transformations in this upper-crustal zone, and has documented their importance in governing fault mechanical behavior [*Schleicher et al.*, 2010; *Si et al.*, 2014; *Warr et al.*, 2014; *Kameda et al.*, 2015] and their utility as deformation geochronometers [*Haines and van der Pluijm*, 2008; *Zwingmann et al.*, 2010; *Hetzel et al.*, 2013; *Bense et al.*, 2014; *Hnat and van der Pluijm*, 2014; *Mancktelow et al.*, 2015]. The clay mineral illite, specifically, has garnered attention due to structurally bound K, O, and H in its lattice, the fact that it forms at low

temperatures, and that we can differentiate between detrital and authigenic populations of the mineral [e.g., *Hetzel et al*., 2013]. Integral to this discussion is the presence and circulation of a fluid that acts as the agent of mineralization and that can govern mechanics; the composition of this fluid acts as an added control on the evolving character of a fault zone [*Wintsch*, 1995; *Mulch et al*., 2006; *Faulkner et al*., 2010]. Constraints on mineralizing fluid composition allow for a more thorough understanding of fault zone maturation processes throughout the displacement cycle, and can also have implications for fault-compartmentalized hydrocarbon reservoir and fault-hosted metal deposit formation and extraction, earthquake risk assessment, and other physico-chemical processes of the brittle crust [*Simpson and Wintsch*, 1989; *Leveille et al*., 1997; *Berger et al*., 2003; *Agosta et al*., 2008].

Results by *Fitz-Díaz et al*. [2014] corroborate the longstanding hypothesis that the oxygen isotope composition of a fluid in the subsurface can equilibrate with the host rock before low-temperature illite authigenesis occurs, but that the absence of hydrogen in most rock-forming phases allows the authigenic minerals to retain a memory of the fluid's original hydrogen isotopic composition [*Criss and Taylor*, 1986; *Sheppard*, 1986]. This is true in the upper crust and as deep as the brittle-plastic transition [e.g., *Mulch et al*., 2004; *Mulch and Chamberlain*, 2007; *Gébelin et al*., 2012; *Campani et al*., 2012]. For this reason, we focus on the hydrogen composition of neoformed clay minerals in this study.

Given the common mixture of detrital and authigenic illite in natural fault rocks, we adapted the illite age analysis (IAA) approach toward characterizing the hydrogen isotopic composition of fluids present in the upper-crustal environment during active deformation. This represents a novel advance in our ability to constrain the formation conditions of authigenic clays. Key to our approach is the integration with dating to ascertain the timing of mineralizing fluids of samples obtained along the long-lived North Anatolian Keirogen (NAK) in which the North Anatolian Fault (NAF) currently resides.

2. Methodologies

The fluid fingerprinting methodology described below is based on the premise that our ability to physically isolate authigenic material from natural rock samples is limited to cases where no detrital clay is present. By separating a single sample into several size fractions that comprise quantifiable ratios of authigenic to detrital material, extrapolation to pure end-member phases is possible using a mixing line [*van der Pluijm et al*., 2001]. This methodology is used in illite age analysis (IAA) with a well ordered, higher temperature illite polytype ($2M_1$) representing the detrital population, and a more disordered, lower temperature illite polytype ($1M_d$) representing the authigenic illite populations. Our approach similarly requires use of grain-size separation and polytype quantification toward hydrogen isotope analysis.

Samples used in this study were characterized by X-ray diffraction (XRD) for mineralogy and polytypism, $^{40}Ar/^{39}Ar$ radiometric dating using the IAA method, all at the University of Michigan, and by continuous flow isotope ratio mass spectrometry for hydrogen isotope compositions at the Joint Stable Isotope Facility at Goethe University Frankfurt.

2.1. Sample Preparation

Samples were collected in northern Turkey at eight sites in four different locations along the surface trend of today's NAF representing an aerial extent of >750 km (Figure 1). Limited by suitable outcrop, two of the locations are on the west and the other two are on the eastern part of the North Anatolian Fault Zone. In the lab, gouge samples were hand-crushed in an agate mortar, repeatedly washed with distilled water to remove salts, and placed in an ultrasonic bath ~15 min to disaggregate and deflocculate clay minerals. The samples containing illite were centrifuged according to Stoke's Law to separate each sample into four different size fractions: 2.0–1.0 μm (coarse), 1.0–0.2 μm (medium), 0.2–0.05 μm (fine), and <0.05 μm (very fine). Aliquots were split for $^{40}Ar/^{39}Ar$ geochronology and isotope measurements before chemical treatment, as the effects of acid treatment on the Ar and H activity in poorly ordered, fine-grained clay minerals are not well understood. These untreated aliquots were used for isotope measurements, while the remaining material was treated for XRD characterization as follows: samples containing carbonate minerals were treated with 1 N HCl at 50°C for 1 h to eliminate peak overlap in X-ray patterns. Oriented powder mounts of each size fraction were prepared on glass slides with a sample density of 5 mg/cm^2.

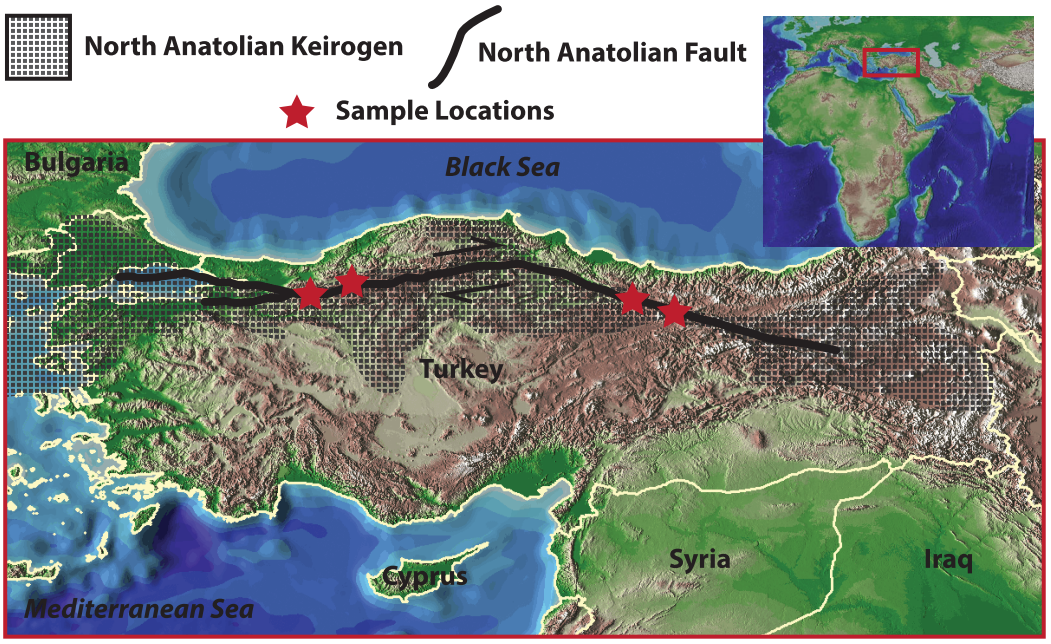

Figure 1. Regional map of Turkey showing sample locations in the North Anatolian Keirogen that includes today's North Anatolian Fault.

Random powder mounts of each size fraction were prepared by the side-loading method of *Moore and Reynolds* [1997].

2.2. X-Ray Diffraction

X-ray diffraction of both oriented samples (used for mineral identification) and randomly oriented samples (used for polytype quantification) was conducted at the Central Campus Electron Microbeam Analysis Laboratory at the University of Michigan. Measurements were taken on a Rigaku Ultima IV diffractometer with CuKα radiation operated in Bragg-Brentano geometry at 40 kV and 44 mA. Oriented slides were measured both in air-dried conditions and after ethylene glycolation from 2 to 80°2θ for mineralogic characterization. Randomly oriented mounts were measured from 16 to 44°2θ for polytype quantification. Less than 2 μm phases common to fault rock include kaolinite, smectite, chlorite, illite, and metal oxides. Other contaminants include feldspar and quartz. Care was taken to avoid samples with even minor amounts of K-feldspar for Ar dating. Samples/size fractions containing illite and $<$5 wt % other phases were selected for isotopic analysis (mineral proportions were assessed qualitatively, based on full-width-half-maximum and peak area measurements of prominent mineral peaks).

2.3. Polytype Quantification

Previous studies (for review, see *van der Pluijm and Hall* [2014]) using illite dating involved the synthetic XRD pattern calculator WILDFIRE© [*Reynolds*, 1993] to generate end-member polytypes, which were mixed to match the pattern of the natural sample toward quantifying its $1M_d/2M_1$ ratio. This application introduces complexity into the quantification due to the array of machine parameters that must be carefully constrained and inserted into the model. We avoid such complications in this study by utilizing natural samples of $2M_1$ and $1M_d$ illite as end-member standards, measured at the same grain size and with the same machine parameters as the natural samples of interest [*Haines and van der Pluijm*, 2008]. Standards used were the $2M_1$ muscovite from the Owl Creek pegmatite (Wind River Mtns.) and the Clay Mineral Society 1Mt-1 $1M_d$ illite standard [*Hower and Mowatt*, 1966]. These standard materials were processed in the same manner as the natural samples. We noticed that the use of clay standards as end-members allows for better resolution of pattern matches and reduces error, as many effects of machine calibration are eliminated. Polytype quantification errors are estimated at ±2–3%. Figure 2 is an example of illite polytype quantification, using sample RES4-1. The results show that the four size fractions derived from RES4-1 have various $1M_d/2M_1$ ratios, and that these ratios systematically correlate with grain size.

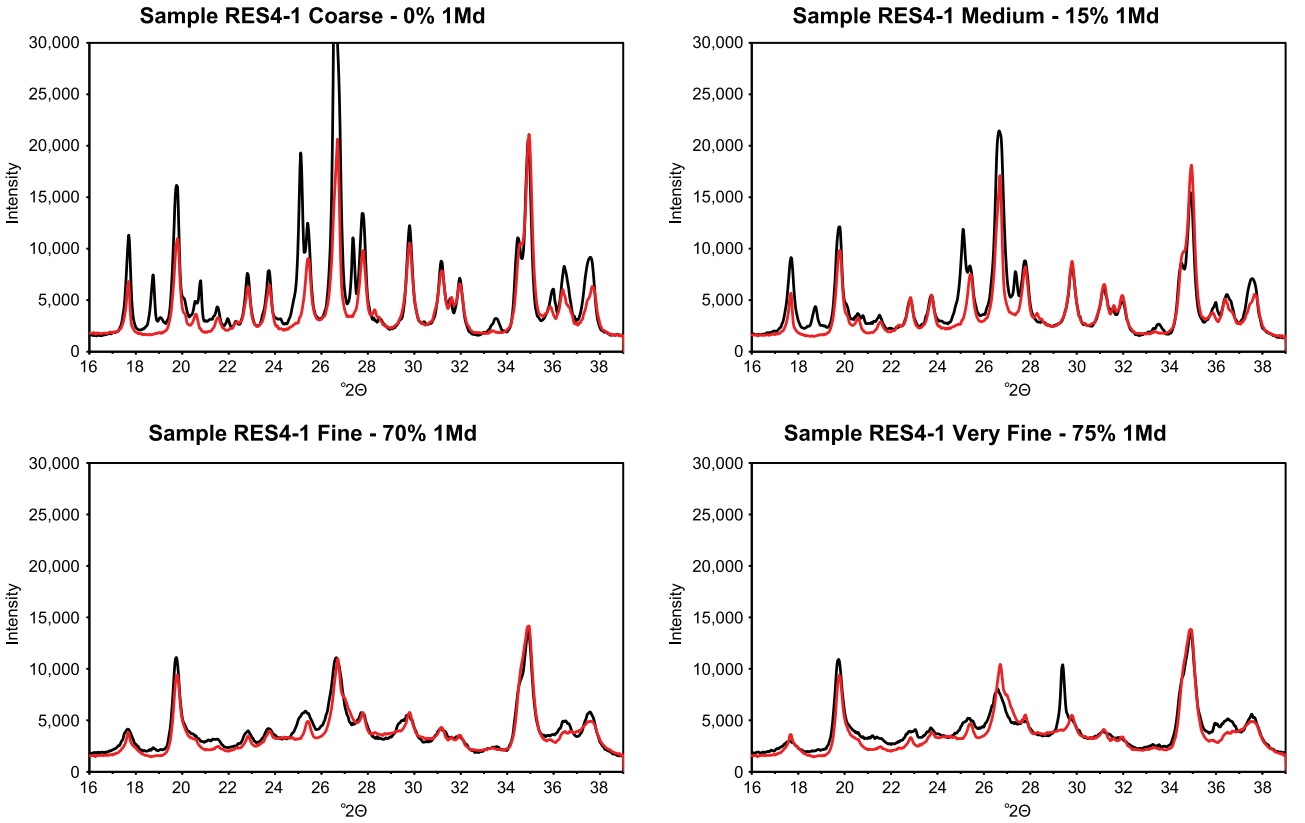

Figure 2. X-ray diffractograms used for polytype quantification of the four size fractions of sample RES4-1. The black pattern is the natural sample and the red pattern is the synthetic match created by mixing the end-member $2M_1$ and $1M_d$ polytype standards. $1M_d/2M_1$ ratios systematically increase with decreasing grain size, indicating an increased abundance of authigenic minerals in the finer fractions.

2.4. Isotopic Analysis

2.4.1. $^{40}Ar/^{39}Ar$ Radiometric Dating

$^{40}Ar/^{39}Ar$ geochronology was conducted by the Noble Gas Laboratory at the University of Michigan using the encapsulation method. The small crystallite size of clay minerals increases recoil during irradiation. Mixed age populations combined with this recoil effect typically lead to degassing spectra and ages that are not defined by plateaus. Encapsulation in quartz tubes during irradiation captures the released argon, which is then measured in bulk, circumventing the problem of recoil [*Dong et al.*, 1995]. Mean illite crystallite size was calculated to be 10–20 nm for dated samples, as obtained by means of the Scherrer equation [*Moore and Reynolds*, 1997]. This crystallite size is used to determine whether the total gas or retention age is appropriate, and for these samples total gas age is used. Note that Ar age errors are a fraction of a percent, but that extrapolated ages incorporate the greater error (2–3%) of polytype characterization, resulting in a larger age error than typical for Ar dating only. See *van der Pluijm and Hall* [2014] for a recent overview of this method.

2.4.2. Hydrogen Isotopic Analysis

About 1 mg of dried sample material was wrapped into Ag foil and kept overnight at 200°C under vacuum. Samples were rapidly transferred to a zero-blank autosampler in a stainless steel tray and the autosampler was immediately purged with helium gas to avoid rehydration with ambient air moisture. δD values were measured at the Joint Goethe University—BiK-F Stable Isotope Facility Frankfurt using a ThermoFinnigan MAT 253 mass spectrometer in continuous flow mode coupled to a high temperature conversion elemental analyzer (TC-EA). In-house and three international standards were run with the samples and yielded $\delta D = -64.8‰$ (NBS30 biotite), $\delta D = -117.9‰$ (NBS22 oil), and $\delta D = -103.2‰$ (CH7 polyethylene foil). Standards were run in-line with unknowns and reproduced with an error below $\pm 2‰$. All δD values are reported relative to standard mean ocean water (VSMOW).

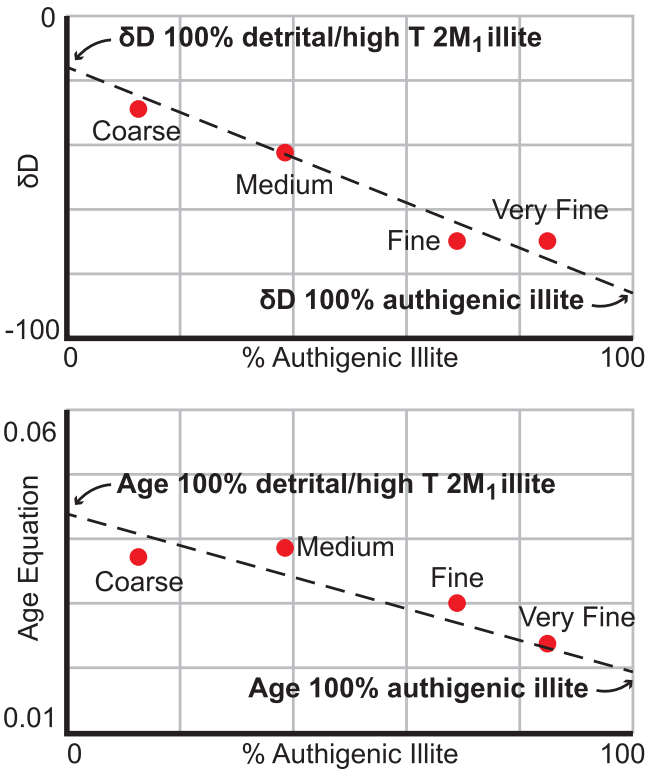

Figure 3. Schematic mixing diagrams plotting size fractions of a single sample in terms of their isotopic composition and % authigenic material. Data are fitted with a regression method; the lower and upper intercepts give values of pure end-member compositions.

2.5. Mixing Plots and Isotopic Model

The key step in our methodology combines the results from multiple grain-size fractions into two relations: one calculates δD for end-member authigenic and detrital illite, and the second constrains their ages. By plotting each size fraction of a sample in terms of the % authigenic illite and isotopic composition, and fitting these data with a York-type regression [*Mahon*, 1996], the intercepts of these lines are extrapolated end-member isotopic values. This is summarized in the idealized mixing plots in Figure 3. The high correlation of the data (R^2 often exceeds 0.9) indicates several important features. First, there are mixtures of two populations of illite in the sample. The line would be horizontal if there was a single population or if multiple populations had undergone postcrystallization isotopic reequilibration. More than two populations of illite would not plot on a linear trend unless all fractions fortuitously contained each population in the exact ratio across grain sizes, which is unlikely due to the mechanical mixing of each sample. Second, hydrogen and argon are not influenced by grain-size dependent diffusion at the temperatures to which these samples have been subjected. If diffusion was occurring, the line would be parabolic, with the smaller grain sizes being more affected than the larger grain sizes, because of changing surface area to volume ratios across the size spectrum. This precludes an argument that a single clay population incompletely experienced isotopic reequilibration to create the mixing line. Finally, we note that the minerals were never subjected to pressure/temperature conditions that exceeded their formation, as the material would have undergone recrystallization and would not exist in two distinct polytypes [*Morad et al.*, 2009]. These characteristics are consistent with an upper-crustal origin and shallow exhumation of the rocks.

3. Application: The North Anatolian Keirogen

3.1. Geological Setting and Sample Description

The tectonic evolution of Northern Turkey has a complex, prolonged history of subduction, terrane accretion, rifting, and escape tectonics. *Şengör and Yilmaz* [1981] describe its development in two phases, defined by the evolution of the Paleo-Tethys and Neo-Tethys Oceans. Phase one: Pangean rifting in the Permian separated Laurasia from Gondwana by the opening of the Paleo-Tethys Ocean. This was subsequently closed by south-dipping subduction underneath the Cimmerian ribbon continent that originated from northern Gondwana. Phase two: the rifting of the Cimmerian Continent from Gondwana opened the Neo-Tethys Ocean. Several terranes of various origins, located in the Neo-Tethys, were accreted to the Eurasian Plate by a series of north-dipping, Cenozoic-aged subduction zones and thrust belts. This convergence marked the closure of the Neo-Tethys, and culminated with the collision of the Arabian Plate with Eurasia in the Miocene (13–11 Ma), initiating the escape tectonic regime—facilitated by the NAF and other faults—

Table 1. Sample Details

Sample ID	Location (UTM)	Mineralogy (<2 μm Fraction)[a]	Used in Study?
G3	4504770, 0379001	Cal	No
G1	4516933, 0428609	Qtz, I, Chl, Kln, Fsp	Yes
G2	4516933, 0428609	Qtz, Cal, I, Fsp, Chl	Yes
KSL	4467014, 0372347	Chl, I, Qtz, Cal, S, Fsp	Yes
KHS2	4458930, 0401524	Qtz, Cal, Chl, Fsp, P	No
RES4-1	4461672, 0391997	Qtz, Chl, I, Fsp	Yes
KO1	4456161, 0410545	Fsp, Cal, Qtz, Py, Chl, S	No
KO3	4456161, 0410545	Fsp, Py	No

[a]Qtz = quartz, I = illite, Chl = chlorite, Kln = kaolinite, Fsp = feldspar, Py = pyrite, Cal = calcite, S = smectite.

that has dominated until the present time [*Tapponnier et al*., 1982; *Şengör*, 1985; *Bozkurt and Mittwede*, 2001; *Şengör et al*., 2005, 2014].

This history illustrates that the area currently occupied by the NAF has been a long-lived tectonic zone since the Late Paleozoic, and it has experienced many and varied deformation events. We capture that prolonged history by using the term North Anatolian Keirogen (NAK), which includes all areas of current deformation in northern Turkey, as well as all underlying Tethyside accretionary complexes [*Şengör and Natal'in*, 1996; *Şengör et al*., 2005]. Further evidence of a prolonged deformation history is provided by the studies of *Uysal et al*. [2006] and *Mutlu et al*. [2010] that obtained K-Ar and Rb-Sr ages of fault rocks with ages from the Paleocene to the Miocene in locations along the trace of today's North Anatolian Fault (NAF). Samples of this study are from locations similar to that of *Uysal et al*. [2006] and *Mutlu et al*. [2010]. The contrasting results of this paper and those—both from a clay mineralogy perspective and an isotopic compositional perspective—can be reconciled by (i) the fact that there are likely faults of various origin and age in the same locality and samples of this study could be different from those of the other studies, or (ii) that if the refined method described in this work was applied to the isotopic results of the other studies, the apparent differences would likely be resolved.

Eight fault gouge samples were collected for this study along the surface trace of the NAF (Figure 1), spanning >750 km eastward of Istanbul. About 0.5–1 kg of sample was collected below the immediate surface to reduce the influence of surface contamination. Samples are typical fault zone clay gouge that is fine-grained, of various color, and friable. Sample G3 is from a carbonate-cemented conglomerate exposed 1 km south of Sultanbeyli village of the city of Bolu. Samples G1 and G2 were collected from the metamorphic rocks on the Bolu-Gerede road. Sample KSL is located near the town Koyulhisar. At this location, the fault gouge sample was taken from a landslide zone comprising interbedded sandstone and shale units. Sample KHS was collected from intensely altered peridotite unit on a roadcut between the towns of Koyulhisar and Resadiye. Sample RES4-1 is from the ultramafic units between sampling locations of samples KSL and KHS. The last two sampling sites, namely KO1 and KO3, are taken from peridotites located along the Kelkit River. Further sample description details and structural context can be found in *Uysal et al*. [2006] and *Mutlu et al*. [2010], which use material from the same locations. Sample location and mineralogic characterizations are listed in Table 1. Only size fractions from samples G1, G2, KSL, and RES4-1 met the criteria for isotopic investigation by containing mostly illite and <5% contaminating phases; the four other samples include significant chlorite and other phases, or contain insufficient illite. Illite in the selected samples occurs both in discrete diffracting domains, as well as interlayered with smectite. The illite-smectite of these samples was remarkably similar between samples, and was evaluated based on 002/003 peak position (d = 4.92–5.04 Å) which indicates that it has long-range ordering ($R \geq 3$) and is illite rich (>90%) [*Moore and Reynolds*, 1997].

3.2. Hydrogen Isotope Results

The results of hydrogen isotopic analysis for the samples investigated, as well as their polytype quantifications, are reported in Table 2. The very fine fraction of samples G1 and KSL did not contain enough illite to model the proportions of detrital and authigenic populations above the noise of small crystallite size peak broadening, background radiation, and contaminating phases, and were therefore omitted. The results of the analyses for samples G1 and G2 are combined because they were collected at the same locality and are otherwise indistinguishable.

Figure 4 displays mixing plots for three sites, showing the success of our approach. Authigenic endmember δD compositions are $-89 \pm 3‰$, $-90 \pm 2‰$, and $-97 \pm 2‰$ for samples KSL, RES4-1, and G1G2, respectively. This range of values is restricted, and implies a common fluid origin for all authigenic populations analyzed, regardless of location.

Table 2. Hydrogen Isotope and Polytype Quantification Results

Sample ID	2.0–1.0 μm	1.0–0.2 μm	0.2–0.05 μm	<0.05 μm
δD (‰, VSMOW)				
G1	−78, −80	−87	−94	−70
G2	−64, −69	−68	−71	−74, −75
RES4-1	−66	−67	−77	−83
KSL	−68	−76	−88	−88
% Authigenic Illite				
G1	50	70	85	
G2	5	15	35	55
RES4-1	0	15	70	75
KSL	50	75	95	

A crystallization temperature can be estimated by various methods in order to calculate δD fluid compositions. *Maden et al*. [2014] calculated a geothermal gradient for the Eastern Anatolian Plateau of 32.2°C/km. Unpublished fault gouge data from samples from the Rwenzori Mountains of East Africa indicate a minimum depth of 3–5 km is needed for authigenesis to occur (S. Haines, personal communication, 2015). This indicates a growth window of ~100–150°C for authigenic minerals. Alternatively, using the smectite-to-illite kinetic reaction model of *Huang et al*. [1993], and assuming a typical [K^+] of 200 ppm and growth time of 1 Ma, we calculate a temperature of formation of ~130°C. This model assumes the likely progression from an intermediate smectite phase [*Boles and Franks*, 1979; *Hower et al*., 1976]. A third estimate considers the long range ($R \geq 3$) ordering pattern of I/S interlayers. The minimum temperature needed to achieve this ordering structure in burial sedimentary basin environments characterized by lower [K^+] is 170°C (*Pollastro*, 1993). Therefore, using a temperature window of 100–150°C and the illite fractionation equation of *Capuano* [1992], calculated δD values for the water from which illite precipitated range from $-59‰$ to $-83‰$.

Detrital end-member δD compositions are $-45 \pm 13‰$, $-60 \pm 6‰$, and $-64 \pm 6‰$ for samples KSL, RES4-1, and G1G2, respectively. These values fall well into the range of muscovite δD values commonly observed in metamorphic rocks. A similar argument as above follows for the detrital populations, that the restricted range of values indicates a common fluid origin for each sample analyzed. The formation temperature for well-ordered $2M_1$ illite is above 300°C [*Frey*, 1987]. Using 300°C as a minimum temperature, and the muscovite fractionation equation of *Suzuoki and Epstein* [1976], δD values of the fluid from which the detrital population of micas precipitated are calculated as $-27‰$ to $-45‰$. The gap of $15‰$ between detrital and authigenic phases is significant and would represent an unlikely shift of almost 20° in latitude if these samples were precipitated at surface conditions and latitudinal isotope gradients in precipitation were wholly responsible for setting δD of meteoric water.

3.3. Illite Dating Results

In order to distinguish between ancient fluid mineralization and modern weathering, two samples were selected for dating. Figure 5 shows the combined results of illite dating using eight size fractions. Sample G2, collected from the western portion of the fault, near the city Gerede, yields an authigenic end-member age of 41.4 ± 3.4 Ma. Sample RES4-1, collected from the eastern portion of the fault near the city of Resadiye, yielded a younger, authigenic end-member age of 24.6 ± 1.6 Ma. Also, both samples yield detrital end-member ages of ~96 Ma (95.8 ± 7.7 Ma for sample G2 and 96.5 ± 3.8 Ma for sample RES4-1), indicating a common history for detrital material that is a significant distance apart today.

4. Discussion and Conclusions

There is a clear compositional demarcation between fluids from which the end-member illite/mica populations precipitated (Figure 6). Fluids associated with authigenic mineralization occupy the range of modern-day precipitation values [*Schemmel et al*., 2013], whereas the fluid associated with detrital minerals is in the range of values that are reported from various metamorphic terranes adjacent to the fault zone [*Bozkaya et al*., 2007; *Canbaz and Gökce*, 2014; *Satir and Taubald*, 2001].

The main factors that may influence the isotopic composition of meteoric fluids in faults and shear zones include climate, altitude, and latitude. For example, Early Eocene global climate has been inferred from proxy data to be the warmest period during the Cenozoic, with deep ocean water temperature ~12°C warmer than current temperatures, and tropical conditions that extended 10–12° latitude poleward of their present positions [*Douglas and Woodruff*, 1981; *Zachos et al*., 2008]. These, and lesser extremes since that time, do not significantly affect our distinction between authigenic fluid and metamorphic fluid. The NAK has experienced little vertical deformation or exhumation since the Miocene, and occupied a broad, low

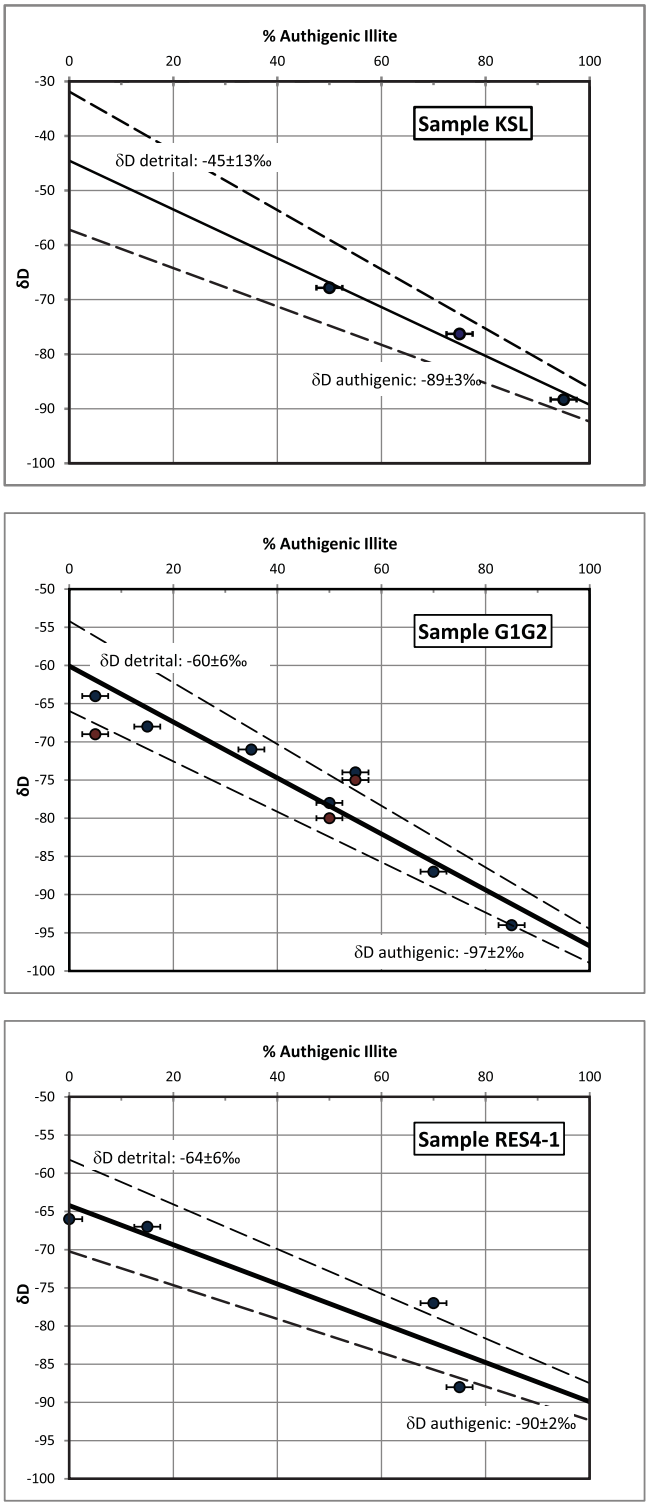

Figure 4. Mixing line diagrams plotting measured δD composition of illite versus % authigenic illite. Data points each represent a single size fraction of sample; ratios of illite polytype populations vary among the multiple size fractions of the sample. This data is fitted with a York-type regression line (solid line) with standard error envelopes (dashed lines). Duplicate measurements not used in regression analysis are displayed in red.

valley for much of its ~1200 km trace [*Koons et al.*, 2003]. Stable isotope studies addressing the role of the Pontide Mountains in controlling precipitation patterns (and associated change in δD of precipitation) are scarce. However, there is increasing stable isotope evidence that the Pontide Mountains did not influence isotope in precipitation patterns at least as far back as the Oligocene [*Mazzini et al.*, 2013; *Lüdecke et al.*, 2013]. The latitude of the NAK has been essentially unchanged throughout the Cenozoic, and has been defined by the southern extent of the stable Eurasian landmass; the orogenic suture zone has likely moved less than 4° latitude since the Paleocene [*Van der Voo*, 1993], with the greatest amount of depletion attributed to this latitudinal change of $<6‰$. Thus, we conclude that climate, elevation and latitude do not vary enough since the Miocene to affect our conclusions about the origins of distinct fluid sources in the area.

Using the nature and ages of mineralization, three fluid flow events can be recognized. The timing and composition of the oldest event is constrained by the detrital end-member populations of the samples at ~96 Ma, with a paleofluid that was metamorphic in nature and produced $2M_1$ illite. These clays were subsequently incorporated into the modern NAF and are today preserved in samples located >400 km apart. We also note that this age is remarkably similar to the age (95–90 Ma) of metamorphic soles of ophiolites that directly overly Eurasian crust and mark the suture between Sakarya (a Eurasian terrane) and the Anatolide-Tauride Block that makes up a large portion of modern Turkey [*van Hinsbergen et al.*, 2010; *Gülyüz et al.*, 2013]. We surmise that during the tectonic emplacement of these terranes, metamorphic fluids were generated by dehydration reactions. These processes, in turn, influenced upper-crustal permeability and porosity structures,

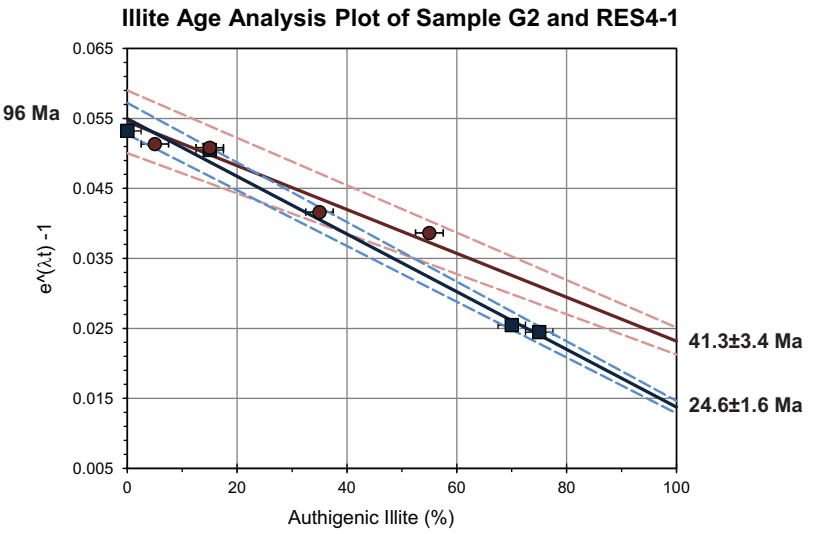

Figure 5. Illite dating plot of samples G2 (red) and RES4-1 (blue). The diagram plots age (in Ar-Ar age equation form) versus % authigenic illite. The authigenic mineralization age of sample G2 is 41.4 ± 3.4 Ma and of sample RES4-1 is 24.6 ± 1.6 Ma. Detrital mineralization ages of the two samples are the same within error; G2 is 95.8 ± 7.7 Ma and RES4-1 is 96.5 ± 3.8 Ma.

and initiated mineralization series that included illite.

The two younger events record meteoric fluid activity in the upper several kilometers of the crust. The depth range of $1M_d$ crystallization is dependent on the geotherm, and is typically constrained to be <4–5 km from the surface [*Hower et al.*, 1976]. The timing of the event on the west side of the area is ~41 Ma. During the mid-Eocene, arc magmatism and associated bentonite deposition continued in the NAK—bentonites are commonly associated with $1M_d$ illite formation [*Pevear*, 1999]. Furthermore, fold-and-thrust belt formation occurred in this time period, providing pathways for fault-related fluid flow and clay generation. The event on the east side of the sampling area is ~25 Ma. Late Oligocene deformation included the transport and emplacement of several nappes and crystalline massifs along southerly imbricated detachments [*Şengör and Yilmaz*, 1981]. Volcanism was restricted to a smaller region, and the initiation of today's North Anatolian Fault was only a few million years away. Regardless of the varied tectonic environments, our isotopic results show that ancient fluids with compositions similar to that of modern-day precipitation have been circulating in the upper crust of the NAK since Early Cenozoic time.

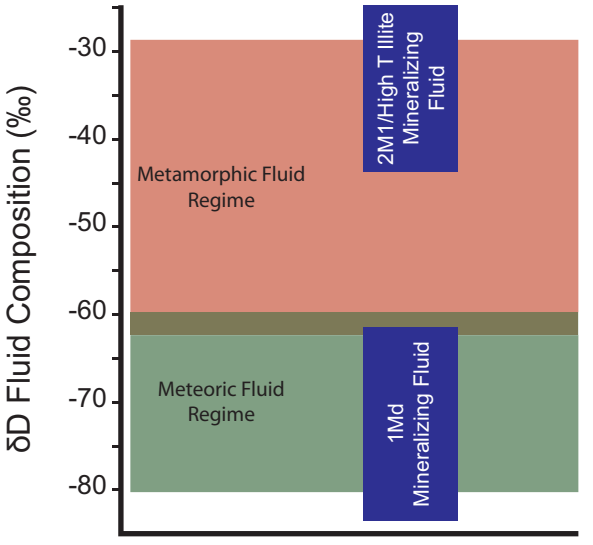

Figure 6. Comparison of δD fluid values of this study (blue) with fluids of metamorphic origin adjacent the fault (red) and modern-day precipitation (green) [*Satir and Taubald*, 2001; *Bozkaya et al.*, 2007; *Schemmel et al.*, 2013; *Canbaz and Gökce*, 2014]. Measured mineral δD values from referenced sources were converted to fluid values based on temperatures, and were converted to VSMOW for comparison.

Our dating shows that clay gouge present in today's North Anatolian Fault is older than modern strike-slip fault initiation. We conclude that older Cenozoic deformation and associated clay formation created zones of weakness in the area that the present-day NAF continues to exploit (Figure 7). This is consistent with various studies indicating across-fault compositional, viscosity, and age differences that point toward large-scale, deep discontinuities between allochthonous terranes of the NAK [*Şengör et al.*, 2005; *Bozkurt and Mittwede*, 2001; *Zattin et al.*, 2010; *Fichtner et al.*, 2013; *Yamasaki et al.*, 2014]. As the nascent NAF propagated through Northern Turkey during a shift from subduction-dominated tectonics to an escape tectonics regime in the Miocene [*Şengör et al.*, 2005], it navigated the terrane aggregate of the region and preferentially utilized weak, clay-rich zones that had been generated during earlier deformation.

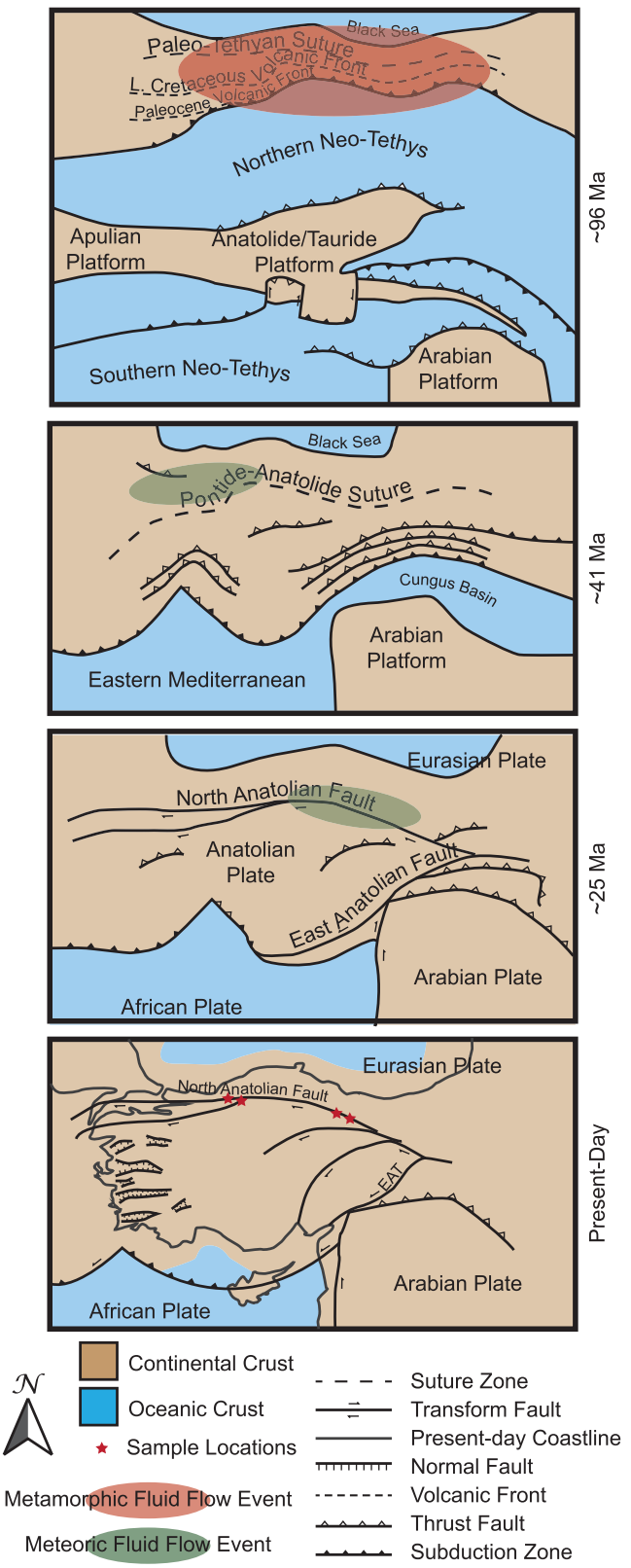

Figure 7. Paleogeographic maps since the late Cretaceous time showing multiple fluid flow/clay mineralization events and illite-bearing sample locations related to tectonic activity in the North Anatolian Keirogen. Maps adapted from *Şengör and Yilmaz* [1981].

Using hydrogen isotopes of clay size fractions for fluid source characterization and associated dating of neoformed and detrital illite, we are able to constrain the nature of mineralizing paleofluids and the timing of fluid circulation pulses within the North Anatolian Keirogen. Our method resolves the complications from mixed sample populations with extremely fine grain sizes, so has potential for application in many other areas, as illitic clays are common in deformation zones. Illite is a robust recorder of formation conditions, preserving a rich source of information about the type, timing and nature of fluids that are associated with regional deformation.

Acknowledgments

Research was supported by the US National Science Foundation EAR 1118704 (BvdP) and the University of Michigan Turner Fund (AB). AM acknowledges support through the US National Science Foundation Continental Dynamics CAT project. We thank Chris Hall (Michigan) for Ar dating, J. Fiebig (Frankfurt) for laboratory support, and Volkan Karabacak (Eskişehir Osmangazi University) for field support. This manuscript was improved by comments from Cin-Ty Lee and an anonymous reviewer. Data used in this study are included in the supporting information.

References

Agosta, F., A. Mulch, C. P. Chamberlain, and A. Aydin (2008), Geochemical traces of CO_2-rich fluid flow along normal faults in central Italy, *Geophys. J. Int.*, *174*, 758–770, doi:10.1111/j.1365-246X.2008.03792.x.

Bense, F. A., K. Wemmer, S. Löbens, and S. Siegesmund (2014), Fault gouge analyses: K-Ar illite dating, clay mineralogy and tectonic significance—A study from the Sierras Pampeanas, Argentina, *Int. J. Earth Sci.*, *103*(1), 189–218, doi:10.1007/s00531-013-0956-7.

Berger, B. R., J. V. Tingley, and L. J. Drew (2003), Structural localization and origin of compartmentalized fluid flow, Comstock Lode, Virginia City, Nevada, *Econ. Geol.*, *98*(2), 387–408, doi:10.2113/gsecongeo.98.2.387.

Boles, J., and S. Franks (1979), Clay diagenesis in Wilcox sandstones of southwest Texas: Implications of smectite diagenesis on sandstone cementation, *J. Sediment. Petrol.*, *49*(1), 55–70, doi:10.1306/212F76BC-2B24-11D7-8648000102C1865D.

Bozkaya, Ö., H. Yalçin, Z. Başibüyük, and G. Bozkaya (2007), Metamorphic-hosted pyrophyllite and dickite occurrences from the hydrous Al-silicate deposits of the Malatya-Pütürge region, central eastern Anatolia, Turkey, *Clays Clay Miner.*, *55*(4), 423–442, doi:10.1346/CCMN.2007.0550409.

Bozkurt, E., and S. K. Mittwede (2001), Introduction to the geology of Turkey—A synthesis, *Int. Geol. Rev.*, *43*(7), 578–594, doi:10.1080/00206810109465034.

Bruhn, R. L., W. A. Yonkee, and W. T. Parry (1990), Structural and fluid-chemical properties of seismogenic normal faults, *Tectonophysics*, *175*, 139–157, doi:10.1016/0040-1951(90)90135-U.

Caine, J. S., J. P. Evans, and C. B. Forster (1996), Fault zone architecture and permeability structure, *Geology*, *24*(11), 1025–1028, doi:10.1130/0091-7613(1996)024<1025:FZAAPS>2.3.CO;2.

Campani, M., A. Mulch, O. Kempf, F. Schlunegger, and N. Mancktelow (2012), Miocene paleotopography of the Central Alps, *Earth Planet. Sci. Lett.*, *337–338*, 174–185, doi:10.1016/j.epsl.2012.05.017.

Canbaz, O., and A. Gökce (2014), Microthermometric and stable isotopic (O and H) characteristics of fluid inclusions in the porphyry related Çöpler (İliç—Erzincan) gold deposit, central eastern Turkey, *Cent. Eur. J. Geosci.*, *6*(2), 139–147, doi:10.2478/s13533-012-0173-0.

Capuano, R. (1992), The temperature dependence of hydrogen isotope fractionation between clay minerals and water: Evidence from a geopressured system, *Geochim. Cosmochim. Acta*, *56*, 2547–2554, doi:10.1016/0016-7037(92)90208-Z.

Criss, R. E., and H. P. Taylor (1986), Meteoric-hydrothermal systems, in *Stable Isotopes in High Temperature Geological Processes, Rev. Mineral. Geochem.*, vol. 16, edited by J. W. Valley, H. P. Taylor Jr., and J. R. O'Neil, pp. 373–424, Am. Mineral. Soc., Blacksburg, Va.

Dong, H., C. Hall, D. Peacor, and A. Halliday (1995), Mechanisms of argon retention in clays revealed by laser 40Ar-39Ar dating, *Science*, *267*(5196), 355–359, doi:10.1126/science.267.5196.355.

Douglas, R. G., and F. Woodruff (1981), Deep sea benthic foraminifera, in *The Sea*, vol. 7, edited by C. Emiliani, pp. 1233–1327, Wiley-Interscience, N. Y.

Faulkner, D. R., C. A. L. Jackson, R. J. Lunn, R. W. Schlische, Z. K. Shipton, C. A. J. Wibberley, and M. O. Withjack (2010), A review of recent developments concerning the structure, mechanics and fluid flow properties of fault zones, *J. Struct. Geol.*, *32*, 1557–1575, doi:10.1016/j.jsg.2010.06.009.

Fichtner, A., E. Saygin, T. Taymaz, P. Cupillard, Y. Capdeville, and J. Trampert (2013), The deep structure of the North Anatolian Fault Zone, *Earth Planet. Sci. Lett.*, *373*, 109–117, doi:10.1016/j.epsl.2013.04.027.

Fitz-Díaz, E., A. Camprubí, E. Cienfuegos-Alvarado, P. Morales-Puente, A. M. Schleicher, and B. van der Pluijm (2014), Newly-formed illite preserves fluid sources during folding of shale and limestone rocks; an example from the Mexican Fold-Thrust Belt, *Earth Planet. Sci. Lett.*, *391*, 263–273, doi:10.1016/j.epsl.2013.12.025.

Frey, M. (1987), Very low-grade metamorphism of clastic sedimentary rocks, in *Low Temperature Metamorphism*, edited by M. Frey, pp. 9–58, Chapman and Hall, N. Y.

Gébelin, A., A. Mulch, C. Teyssier, C. P. Chamberlain, and M. Heizler (2012), Coupled basin-detachment systems as paleoaltimetry archives of the western North American Cordillera, *Earth Planet. Sci. Lett.*, *335–336*, 36–47, doi:10.1016/j.epsl.2012.04.029.

Gülyüz, E., N. Kaymakci, M. J. M. Meijers, D. J. J. van Hinsbergen, C. Lefebvre, R. L. M. Vissers, B. W. H. Hendriks, and A. A. Peynircioğlu (2013), Late Eocene evolution of the Çiçekdağı Basin (central Turkey): Syn-sedimentary compression during microcontinent-continent collision in central Anatolia, *Tectonophysics*, *602*, 286–299, doi:10.1016/j.tecto.2012.07.003.

Haines, S. H., and B. A. van der Pluijm (2008), Clay quantification and Ar-Ar dating of synthetic and natural gouge—Application to the Miocene Sierra Mazatán detachment fault, Sonora, Mexico, *J. Struct. Geol.*, *30*, 525–538.

Hetzel, R., H. Zwingmann, A. Mulch, K. Gessner, C. Akal, A. Hampel, T. Güngör, R. Petschick, T. Mikes, and F. Wedin (2013), Spatiotemporal evolution of brittle normal faulting and fluid infiltration in detachment fault systems: A case study from the Menderes Massif, western Turkey, *Tectonics*, *32*, 364–376, doi:10.1002/tect.20031.

Hickman, S., R. Sibson and R. Bruhn (1995), Introduction to special section: Mechanical involvement of fluids in faulting, *J. Geophys. Res.*, *100*(B7), 12,831–12,840, doi:10.1029/95JB01121.

Hnat, J. S., and B. A. van der Pluijm (2014), Fault gouge dating in the Southern Appalachians, USA, *Geol. Soc. Am. Bull.*, *126*(5–6), 639–651, doi:10.1130/B30905.1.

Hower, J., and T. C. Mowatt (1966), The mineralogy of illites and mixed-layer illite/montmorillonites, *Am. Mineral.*, *51*, 825–854.

Hower, J., E. V. Eslinger, M. E. Hower, and E. Perry (1976), Mechanism of burial metamorphism of argillaceous sediment. 1: Mineralogical and chemical evidence, *Geol. Soc. Am. Bull.*, *87*, 725–737, doi:10.1130/0016-7606(1976)87<725:MOBMOA>2.0.CO;2.

Huang, W., J. M. Longo, and D. R. Pevear (1993), An experimentally derived kinetic model for smectite-to-illite conversion and its use as a geothermometer, *Clays Clay Miner.*, *41*(2), 162–177.

Kameda, J., M. Shimizu, K. Ujiie, T. Hirose, M. Ikari, J. Mori, K. Oohashi, and G. Kimura (2015), Pelagic smectite as an important factor in tsunamigenic slip along the Japan Trench, *Geology*, *43*, 155–158, doi:10.1130/G35948.1.

Koons, P., R. Norris, D. Craw, and A. Cooper (2003), Influence of exhumation on the structural evolution of transpressional plate boundaries: An example from the Southern Alps, New Zealand, *Geology*, *31*(1), 3–6, doi:10.1130/0091-7613(2003)031<0003.

Leveille, G. P., R. Knipe, and C. More (1997), Compartmentalization of Rotliegendes gas reservoirs by sealing faults, Jupiter Fields area, southern North Sea, in *Petroleum Geology of the Southern North Sea; Future Potential*, vol. 123, edited by K. Ziegler, P. Turner, and S. R. Daines, pp. 87–104, Geol. Soc., London, doi:10.1144/GSL.SP.1997.123.01.06.

Lüdecke, T., T. Mikes, B. Rojay, M. Cosca, and A. Mulch (2013), Oligo-Miocene paleoenvironment and paleohydrology of Central Anatolian lake basins, *Turk. J. Earth Sci.*, *22*, 793–819, doi:10.3906/yer-1207-11.

Maden, N., A. Aydin, and F. Kadirov (2014), Determination of the crustal and thermal structure of the Erzurum-Horasan-Pasinler Basins (Eastern Türkiye) using gravity and magnetic data, *Pure Appl. Geophys.*, *172*, 1599–1614, doi:10.1007/s00024-014-1001-x.

Mahon, K. (1996), The New "York" regression: Application of an improved statistical method to geochemistry, *Int. Geol. Rev.*, *38*, 293–303, doi:10.1080/00206819709465336.

Mancktelow, N., H. Zwingmann, M. Campani, B. Fügenschuh, and A. Mulch (2015), Timing and conditions of brittle faulting on the Silltal-Brenner Fault Zone, Eastern Alps (Austria), *Swiss J. Geosci.*, doi:10.1007/s00015-015-0179-y.

Mazzini, I., N. Hudackova, P. Joniak, M. Kovacova, T. Mikes, A. Mulch, B. Rojay, S. Lucifora, D. Esu, and I. Soulie-Märsche (2013), Palaeoenvironmental and chronological constraints on the Tuğlu formation (Çankırı Basin, Central Anatolia, Turkey), *Turk. J. Earth Sci.*, *22*, 747–777, doi:10.3906/yer-1207-10.

Moore, D. M., and R. C. J. Reynolds (1997), *X-ray Diffraction and the Identification and Analysis of Clay Minerals*, Oxford Univ. Press, N. Y.

Morad, S., R. Worden, and J. Ketzer (2009), Oxygen and hydrogen isotopic composition of diagenetic clay minerals in sandstones: A review of the data and controls, in *Clay Mineral Cements in Sandstones*, edited by R. Worden and S. Morad, Special publication 34 of the IAS (International association of sedimentologists), pp. 63–91, Wiley-Blackwell, doi:10.1002/9781444304336.ch3.

Mulch, A., and C. P. Chamberlain (2007), Stable isotope paleoaltimetry in orogenic belts—The silicate record in surface and crustal geological archives, *Rev. Mineral. Geochem.*, *66*(1), 89–118, doi:10.2138/rmg.2007.66.4.

Mulch, A., C. Teyssier, M. A. Cosca, O. Vanderhaeghe, and T. W. Vennemann (2004), Reconstructing paleoelevation in eroded orogens, *Geology*, *32*(6), 525–528, doi:10.1130/G20394.1.

Mulch, A., C. Teyssier, M. A. Cosca, and T. W. Vennemann (2006), Thermomechanical analysis of strain localization in a ductile detachment zone, *J. Geophys. Res.*, *111*, B12405, doi:10.1029/2005JB004032.

Mutlu, H., I. T. Uysal, E. Altunel, V. Karabacak, Y. Feng, J. Zhao, and O. Atalay (2010), Rb-Sr systematics of fault gouges from the North Anatolian Fault Zone (Turkey), *J. Struct. Geol.*, *32*, 216–221, doi:10.1016/j.jsg.2009.11.006.

Oliver, J. (1986), Fluids expelled tectonically from orogenic belts: Their role in hydrocarbon migration and other geologic phenomena, *Geology*, *14*(2), 99–102, doi:10.1130/0091-7613(1986)14<99:FETFOB>2.0.CO;2.

Person, M., A. Mulch, C. Teyssier, and Y. Gao (2007), Isotope transport and exchange within metamorphic core complexes, *Am. J. Sci.*, *307*(3), 555–589, doi:10.2475/03.2007.01.

Pevear, D. R. (1999), Illite and hydrocarbon exploration, *Proc. Natl. Acad. Sci. U. S. A.*, *96*(7), 3440–3446, doi:10.1073/pnas.96.7.3440.

Pollastro, R. M. (1993), Considerations and applications of the illite/smectite geothermometer in hydrocarbon-bearing rocks of Miocene to Mississippian age, *Clays Clay Miner.*, *41*(2), 119–133.

Reynolds, R. C. J. (1993), *WILDFIRE—A Computer Program for the Calculation of Three-Dimensional Powder X-Ray Diffraction Patters for Mica Polytypes and their Disordered Variations*, N. H.

Satir, M., and H. Taubald (2001), Hydrogen and oxygen isotope evidence for fluid-rock interactions in the Menderes massif, western Turkey, *Int. J. Earth Sci.*, *89*(4), 812–821, doi:10.1007/s005310000135.

Schemmel, F., T. Mikes, B. Rojay, and A. Mulch (2013), The impact of topography on isotopes in precipitation across the Central Anatolian Plateau (Turkey), *Am. J. Sci.*, *313*(2), 61–80, doi:10.2475/02.2013.01.

Schleicher, A. M., B. A. van der Pluijm, and L. N. Warr (2010), Nanocoatings of clay and creep of the San Andreas fault at Parkfield, California, *Geology*, *38*(7), 667–670, doi:10.1130/G31091.1.

Scholz, C. (1987), Wear and gouge formation in brittle faulting, *Geology*, *15*, 493–495, doi:10.1130/0091-7613(1987)15<493:WAGFIB>2.0.CO;2.

Şengör, A. M. C. (1985), Strike-slip faulting and related basin formation in zones of tectonic escape: Turkey as a case study, *Spec. Publ. SEPM*, *37*, 227–264.

Şengör, A. M. C., and B. A. Natal'in (1996), Palaeotectonics of Asia: Fragments of a synthesis, in *The Tectonic Evolution of Asia, Rubey Colloquium*, edited by A. Yin and M. Harrison, pp. 486–640, Cambridge Univ. Press, Cambridge, U. K.

Şengör, A. M. C., and Y. Yilmaz (1981), Tethyan evolution of Turkey: A plate tectonic approach, *Tectonophysics*, *75*(3–4), 181–241, doi:10.1016/0040-1951(81)90275-4.

Şengör, A. M. C., O. Tüysüz, C. İmren, M. Sakınç, H. Eyidoğan, N. Görür, X. Le Pinchon, and C. Rangin (2005), The North Anatolian Fault: A new look, *Annu. Rev. Earth Planet. Sci.*, *33*, 37–112, doi:10.1146/annurev.earth.32.101802.120415.

Şengör, A. M. C., C. Grall, C. İmren, X. Le Pichon, N. Görür, P. Henry, H. Karabulut, and M. Siyako (2014), The geometry of the North Anatolian transform fault in the Sea of Marmara and its temporal evolution: Implications for the development of intracontinental transform faults, *Can. J. Earth Sci.*, *51*, 222–242, doi:10.1139/cjes-2013-0160.

Sheppard, S. M. F. (1986), Characterization and isotopic variations in natural waters, *Rev. Mineral.*, *16*, 165–183.

Si, J., H. Lia, L. Kuoc, J. Peia, S. Song, and H. Wang (2014), Clay mineral anomalies in the Yingxiu-Beichuan fault zone from the WFSD-1 drilling core and its implication for the faulting mechanism during the 2008 Wenchuan earthquake (Mw 7.9), *Tectonophysics*, *619–620*, 171–178, doi:10.1016/j.tecto.2013.09.022.

Sibson, R. (1977), Fault rocks and fault mechanisms, *J. Geol. Soc. London*, *133*, 191–213, doi:10.1144/gsjgs.133.3.0191.

Sibson, R. H. (1992), Implications of fault-valve behaviour for rupture nucleation and recurrence, *Tectonophysics*, *211*(1–4), 283–293, doi:10.1016/0040-1951(92)90065-E.

Simpson, C., and R. P. Wintsch (1989), Evidence for deformation-induced K-feldspar replacement by myrmekite, *J. Metamorph. Geol.*, *7*, 261–275, doi:10.1111/j.1525-1314.1989.tb00588.x.

Sutherland, R., et al. (2012), Drilling reveals fluid control on architecture and rupture of the Alpine fault, New Zealand, *Geology*, *40*(12), 1143–1146, doi:10.1130/G33614.1.

Suzuoki, T., and S. Epstein (1976), Hydrogen isotope fractionation between OH-bearing minerals and water, *Geochim. Cosmochim. Acta*, *40*(10), 1229–1240, doi:10.1016/0016-7037(76)90158-7.

Tapponnier, P., G. Peltzer, and A. Y. Le Dain (1982), Propagating extrusion tectonics in Asia: New insights from simple experiments with plasticine, *Geology*, *10*, 611–616, doi:10.1130/0091-7613(1982)10<611:PETIAN>2.0.CO;2.

Uysal, I., H. Mutlu, E. Altunel, V. Karabacak, and S. Golding (2006), Clay mineralogical and isotopic (K–Ar, δ18O, δD) constraints on the evolution of the North Anatolian Fault Zone, Turkey, *Earth Planet. Sci. Lett.*, *243*(1–2), 181–194, doi:10.1016/j.epsl.2005.12.025.

van der Pluijm, B., and C. Hall (2014), *Brittle Fault Dating, Encyclopedia of Scientific Dating Methods*, Springer, N. Y.

van der Pluijm, B. A., C. M. Hall, P. Vrolijk, D. R. Pevear, and M. Covey (2001), The dating of shallow faults in the Earth's crust, *Nature*, *412*, 172–174.

Van der Voo, R. (1993), *Paleomagnetism of the Atlantic, Tethys, and Iapetus Oceans*, Cambridge Univ. Press, N. Y.

van Hinsbergen, D., N. Kaymakci, W. Spakman, and T. Torsvik (2010), Reconciling the geological history of western Turkey with plate circuits and mantle tomography, *Earth Planet. Sci. Lett.*, *297*, 674–686, doi:10.1016/j.epsl.2010.07.024.

Warr, L. N., J. Wojatschke, B. M. Carpenter, C. Marone, A. M. Schleicher, and B. A. van der Pluijm (2014), A "slice-and-view" (FIB-SEM) study of clay gouge from the SAFOD creeping section of the San Andreas Fault at ~2.7 km depth, *J. Struct. Geol.*, *69*, 234–244, doi:10.1016/j.jsg.2014.10.006.

Wintsch, R. (1995), Fluid-rock reaction weakening of fault zones, *J. Geophys. Res.*, *100*(B7), 13,021–13,032, doi:10.1029/94JB02622.

Yamasaki, T., T. J. Wright, and G. A. Houseman (2014), Weak ductile shear zone beneath a major strike-slip fault: Inferences from earthquake cycle model constrained by geodetic observations of the western North, *J. Geophys. Res.*, *119*, 3678–3699, doi:10.1002/2013JB010347.

Zachos, J. C., G. R. Dickens, and R. E. Zeebe (2008), An early Cenozoic perspective on greenhouse warming and carbon-cycle dynamics, *Nature*, *451*, 279–283, doi:10.1038/nature06588.

Zattin, M., W. Cavazza, A. I. Okay, I. Federici, M. G. Fellin, A. Pignalosa, and P. Reiners (2010), A precursor of the North Anatolian Fault in the Marmara Sea region, *J. Asian Earth Sci.*, *39*, 97–108, doi:10.1016/j.jseaes.2010.02.014.

Zwingmann, H., N. Mancktelow, M. Antognini, and R. Lucchini (2010), Dating of shallow faults: New constraints from the AlpTransit tunnel site (Switzerland), *Geology*, *38*(6), 487–490, doi:10.1130/G30785.1.